

SHORT REPORT

Nuclear localization of p65 reverses therapy-induced senescence

Sameer Salunkhe^{1,2}, Saket V. Mishra^{1,2}, Jyothi Nair^{1,2}, Sanket Shah^{1,2}, Nilesh Gardi^{2,3}, Rahul Thorat⁴, Debashmita Sarkar^{1,2}, Jacinth Rajendra^{1,2}, Ekjot Kaur^{1,2} and Shilpee Dutt^{1,2,*}

ABSTRACT

Senescence is the arrest of cell proliferation and is a tumor suppressor phenomenon. In a previous study, we have shown that therapy-induced senescence of glioblastoma multiforme (GBM) cells can prevent relapse of GBM tumors. Here, we demonstrate that ciprofloxacin-induced senescence in glioma-derived cell lines and primary glioma cultures is defined by SA- β -gal positivity, a senescence-associated secretory phenotype (SASP), a giant cell (GC) phenotype, increased levels of reactive oxygen species (ROS), γ -H2AX and a senescence-associated gene expression signature, and has three stages of senescence – initiation, pseudo-senescence and permanent senescence. Ciprofloxacin withdrawal during initiation and pseudo-senescence reinitiated proliferation *in vitro* and tumor formation *in vivo*. Importantly, prolonged treatment with ciprofloxacin induced permanent senescence that failed to reverse following ciprofloxacin withdrawal. RNA-seq revealed downregulation of the p65 (RELA) transcription network, as well as incremental expression of SMAD pathway genes from initiation to permanent senescence. Ciprofloxacin withdrawal during initiation and pseudo-senescence, but not permanent senescence, increased the nuclear localization of p65 and escape from ciprofloxacin-induced senescence. By contrast, permanently senescent cells showed loss of nuclear p65 and increased apoptosis. Pharmacological inhibition or genetic knockdown of p65 upheld senescence *in vitro* and inhibited tumor formation *in vivo*. Our study demonstrates that levels of nuclear p65 define the window of reversibility of therapy-induced senescence and that permanent senescence can be induced in GBM cells when the use of senotherapeutics is coupled with p65 inhibitors.

KEY WORDS: Accelerated senescence, Transcription factor p65, RELA, Reactive oxygen species, SMADs, Therapy-induced senescence, Reversible senescence, GBM

INTRODUCTION

Senescence, an irreversible state of cell cycle arrest, can act as a tumor-suppressive program (Lee and Schmitt, 2019). Thus, induction of senescence can be exploited for cancer therapy. Indeed, chemoradiotherapy can induce senescence, i.e. therapy-induced senescence (TIS), in lung, colon and breast cancers, leukemia and glioblastomas (Chang et al., 1999, 2002; Duy et al., 2016; Ewald et al.,

2010; Kaur et al., 2015; Quick and Gewirtz, 2006; Roberson et al., 2005), and was shown to have a favorable outcome in mouse lymphoma and liver cancer models (Schmitt et al., 2002; Xue et al., 2007; Zhang and Yang, 2011).

Senescence-inducing drugs (senotherapeutics) – like CDK4 or CDK6 inhibitors – are effective against several cancers (Geoerger et al., 2017; Goldman et al., 2016; Turner et al., 2015). High-throughput clustered regularly interspaced short palindromic repeats (CRISPR) and chemical genetic screens also identified senescence inducers in cancer cells (Wang et al., 2017). Here, we discovered that ciprofloxacin, an antibiotic belonging to the fluoroquinolone group of antibiotics, induces senescence in glioblastoma. Ciprofloxacin acts by inhibiting topoisomerase II in eukaryotic and bacterial cells (Chen and Liu, 1994; Chen et al., 1996; Kloskowski et al., 2012). Interestingly, ciprofloxacin has also been shown to inhibit growth and induce apoptosis of bladder carcinoma (Seay et al., 1996), osteosarcoma (Miclau et al., 1998), prostate cancer (Aranha et al., 2003) and blood cancer (leukemia) (Somekh et al., 1989). However, these studies lack mechanistic details of how senescence is induced by ciprofloxacin.

Therapy-induced senescent cells were thought to be permanently cell-cycle arrested; however, our data from glioblastomas (Kaur et al., 2020, 2015), and reports that used non-small cell lung, prostate, colon or breast cancers have shown that therapy-induced senescent cells can resume growth and relapse (Saleh et al., 2019; Schmitt, 2018; Ewald et al., 2010; Roberson et al., 2005; Elmore et al., 2005; Ewald and Jarrard, 2012; Passos et al., 2010). Mechanistically, genotoxic stress, telomere shortening or dysfunction, and oncogene activation have been shown to induce senescence (Di Micco et al., 2006; Fumagalli et al., 2012; Herbig and Sedivy, 2006; Passos et al., 2010). However, little is known about the mechanisms that are responsible for reversal of senescence. One report has shown that levels of p16INK4a determine reversibility of oncogene-induced senescence (Beauséjour et al., 2003); yet, the molecular players that enable therapy-induced senescent cells to reverse have, so far, remained elusive.

Here, we show that ciprofloxacin-induced senescence in glioblastoma cells is dynamic and defined by three stages: (1) initiation, (2) pseudo-senescence and (3) permanent senescence. At the different stages, senescent cells showed similar gene expression signatures but distinctive molecular features of cellular senescence. Ciprofloxacin withdrawal during initiation and pseudo-senescence resulted in cells resuming proliferation – giving rise to ‘revertants’ – and thereby causing disease relapse. Mechanistically, the presence of transcription factor p65 (RELA, hereafter referred to as p65) in the nucleus is necessary and sufficient to reverse senescence. Accordingly, p65 inhibitors, when used concomitantly with senotherapeutics, can induce a permanently senescent state of cancer cells, thus preventing recurrence.


RESULTS AND DISCUSSION

Ciprofloxacin induces cytostasis and senescence in glioma cells

We used glioblastoma cell lines (U87 and SF268) and primary cultures derived from primary GBM patient samples (PS1 and PS5)

¹Shilpee Dutt Laboratory, Advanced Centre for Treatment, Research and Education in Cancer, Kharghar, Navi Mumbai, Maharashtra 410210, India. ²Homi Bhabha National Institute, Training School Complex, Anushakti Nagar, Mumbai 400 094, India. ³Department of Medical Oncology, Tata Memorial Hospital, Tata Memorial Centre, Navi Mumbai, Maharashtra 410210, India. ⁴Laboratory Animal Facility, Advanced Centre for Treatment, Research and Education in Cancer Kharghar, Navi Mumbai, Maharashtra 410210, India.

*Author for correspondence (sdutt@actrec.gov.in)

 J.R., 0000-0002-4432-4918; E.K., 0000-0002-7937-6646; S.D., 0000-0003-4217-5127

Handling Editor: David Glover

Received 20 August 2020; Accepted 21 January 2021

to examine the effect of ciprofloxacin on their growth. Initially, MTT assay at 48 h with different ciprofloxacin concentrations showed no effect of ciprofloxacin on the viability of GBM cells (Fig. 1A). However, long-term cell growth assay showed complete cytostasis with 100 $\mu\text{g/ml}$ ciprofloxacin in U87 and SF268 cells until day 15, beyond which cell death was observed. Importantly, ciprofloxacin did not induce cytostasis in the non-tumorigenic epithelial cell line MCF 10A, which was used as a control cell line (Fig. 1B,C), thereby demonstrating a cancer cell-specific cytostatic effect of ciprofloxacin. All subsequent experiments were performed by using 100 $\mu\text{g/ml}$ of ciprofloxacin. Glioma cells treated with ciprofloxacin displayed the morphology of giant cell glioblastoma (GC) with the GC percentage being increased from 15% (day 5), 30–35% (day 10), up to 72–60% (day15). By contrast, no morphological changes were seen in MCF10A cells (Fig. S1A,B). We have previously reported GC formation in glioma cells exposed to gamma radiation (Kaur et al., 2019, 2015, 2016; Rajendra et al., 2018). Since breakdown of actin microfilaments is essential for morphological alterations in cells (Schäfer et al., 1998), we investigated the effect of ciprofloxacin on the organization of actin microfilaments by using F-actin immunofluorescence. Control cells showed a well-defined network of actin filaments. Treatment with ciprofloxacin for 15 days, however, resulted in decreased expression and disrupted organization of the F-actin microfilament network (Fig. S2A). Since ciprofloxacin induced cytostasis with GC morphology, we analyzed cells for senescence by staining for senescence-associated beta-galactosidase (SA- β -gal). In response to treatment with ciprofloxacin, 25, 48 and 90% of U87 cells were positive for SA- β -gal at days 5, 10 and 15, respectively (Fig. 1D). We also found increasing levels of senescence-associated secretory phenotype (SASP) transcripts, i.e. *CXCL8* and *CSF2* (Lawless et al., 2010), in U87 cells treated with ciprofloxacin for the same durations (Fig. 1E). Furthermore, RNA seq analysis of U87 cells treated with ciprofloxacin for 5, 10 or 15 days showed the gene signature for senescence (Fig. 1F). Importantly, although β -gal-positive cells from all treatment days showed the senescence gene signature, we also noticed variations between days (Fig. 1F).

Cellular senescence is linked to DNA damage and increased levels of reactive oxygen species (ROS) (Chen et al., 2007; Colavitti and Finkel, 2005; Ditch and Paull, 2012; Shiloh and Ziv, 2013). We therefore, tested whether DNA damage response (DDR) and ROS play a role in ciprofloxacin-mediated senescence. Compared to controls, ROS levels increased 1.36-fold in U87 at day10, and further to 1.45-fold at day15 (Fig. S2B). Additionally, immunostaining for γ -H2AX and phosphorylated ATM (p-ATM) in U87 indicated DDR in ~80% cells at days 10 and 15 of ciprofloxacin treatment (Fig. 1G). The presence of ROS and DNA damage suggests that both play a crucial role in maintenance of senescence. U87, SF268 and PS5 glioblastoma cells also showed increased apoptosis on day 15 of ciprofloxacin treatment (Fig. S2C).

Withdrawal of ciprofloxacin reverses senescence in a time-dependent manner

To determine the long-term effect of ciprofloxacin on cell proliferation, glioblastoma cell lines and primary cultures were treated with ciprofloxacin for 5, 10 or 15 days. Thereafter, ciprofloxacin was withdrawn; cells were allowed to grow in ciprofloxacin-free medium, and cell numbers were determined every 48 h. Unexpectedly, when exposure to ciprofloxacin was stopped after 5 or 10 days of treatment, senescent cells re-entered the cell cycle and, after growing slowly for 2–3 days, achieved proliferation rates similar to those of control cultures (Fig. 2A and Fig. S3A–C). Importantly, ciprofloxacin

treatment for 15 days rendered cells unable to proliferate upon drug withdrawal and showed cell death within the next 10–15 days. Moreover, non-tumorigenic MCF 10A cells, did not show any change in proliferation with or without ciprofloxacin treatment, or removal after days 5 or 10 (Fig. S3D). To confirm that the senescent cells, indeed, were able to escape senescence and regrow, we sorted cells that had been treated with ciprofloxacin for 10 days into senescent-positive and -negative cells based on their size and autofluorescence, followed by confirmation of senescence by staining for SA- β -gal. When allowed to grow in culture, senescent as well as non-senescent cells were able to proliferate, confirming that senescence initiated by treatment with ciprofloxacin for ≤ 10 days is, indeed, reversible (Fig. 2B). These results were also validated in primary cultures obtained from GBM patients (Fig. S3E).

Nuclear localization of p65 reverses senescence

The fact that we found ciprofloxacin-induced senescence to be reversible up to a certain time point has important clinical implications, as premature termination of a drug on the basis of the senescence phenotype alone might lead to recurrence of the disease. We, therefore, wanted to understand the molecular changes that push reversible senescence to terminal senescence. For this, we performed whole-transcriptome analysis of U87 glioma cells induced for senescence by using ciprofloxacin for 5, 10 or 15 days. Interestingly, the p65 gene network exhibited inverse gene expression profiles – genes upregulated in control U87 cells were downregulated post ciprofloxacin treatment and vice versa (Fig. 2C). p65 is known to control ROS by regulating gene expression of superoxide dismutases (SODs; i.e. SOD1, SOD2, SOD3), glutathione S-transferase pi 1 (GSTP1) and NADPH oxidase NOX2 (also known as CYBB and gp91-phox) (Morgan and Liu, 2011). We analyzed the cellular localization of p65 on different days in the presence of ciprofloxacin and after its removal (immunostaining for p65 was performed 5 days after ciprofloxacin removal) and found p65 in the cytoplasm of senescent U87 cells, whereas its nuclear localization significantly increased with ciprofloxacin withdrawal at day5 and day10 (Fig. 2D). Importantly, at day15 with or without ciprofloxacin, p65 was not localized in nucleus (Fig. 2D). Similar results were obtained in SF268 cells and patient-derived glioblastoma cells (PS1), both of which showed nuclear localization of p65 associated with reversible senescence (Fig. S4A,B). Accordingly, prevention of p65 nuclear translocation should keep the cells senescent. To test this, we used two inhibitors of p65 translocation (anacardic acid and JSH23). Anacardic acid blocks the activity of histone acetyltransferase p300 (also known as EP300), thereby indirectly inhibiting the transport of p65 into the nucleus, whereas JSH23 selectively blocks p65 nuclear translocation. Activity of the inhibitors was confirmed by assessing p65 translocation to the nucleus (Fig. 2E). Indeed, prevention of p65 translocation to the nucleus after treatment with ciprofloxacin combined with p65 inhibitors (anacardic acid or JSH23) resulted in increased numbers of SA- β -gal-positive cells, compared to cells that had been treated with ciprofloxacin for 5 or 10 days, followed by drug removal for 5 days (day5R or day10R, respectively; Fig. 2F). Importantly, cells that remained senescent upon anacardic acid or JSH23 treatment eventually died (data not shown). Furthermore, following inhibition of p65 translocation by anacardic acid or JSH23 treatment on day10, ciprofloxacin-treated cells maintained higher levels of ROS, equivalent to those of day15 ciprofloxacin-treated cells, suggesting that translocation of p65 into the nucleus helps to quench ROS levels. Accordingly, reduced transcript levels of *SOD2* in day10R+anacardic acid and day15 cells compared to those in day10R alone cells confirm these findings. Additionally, levels of NOX4 and

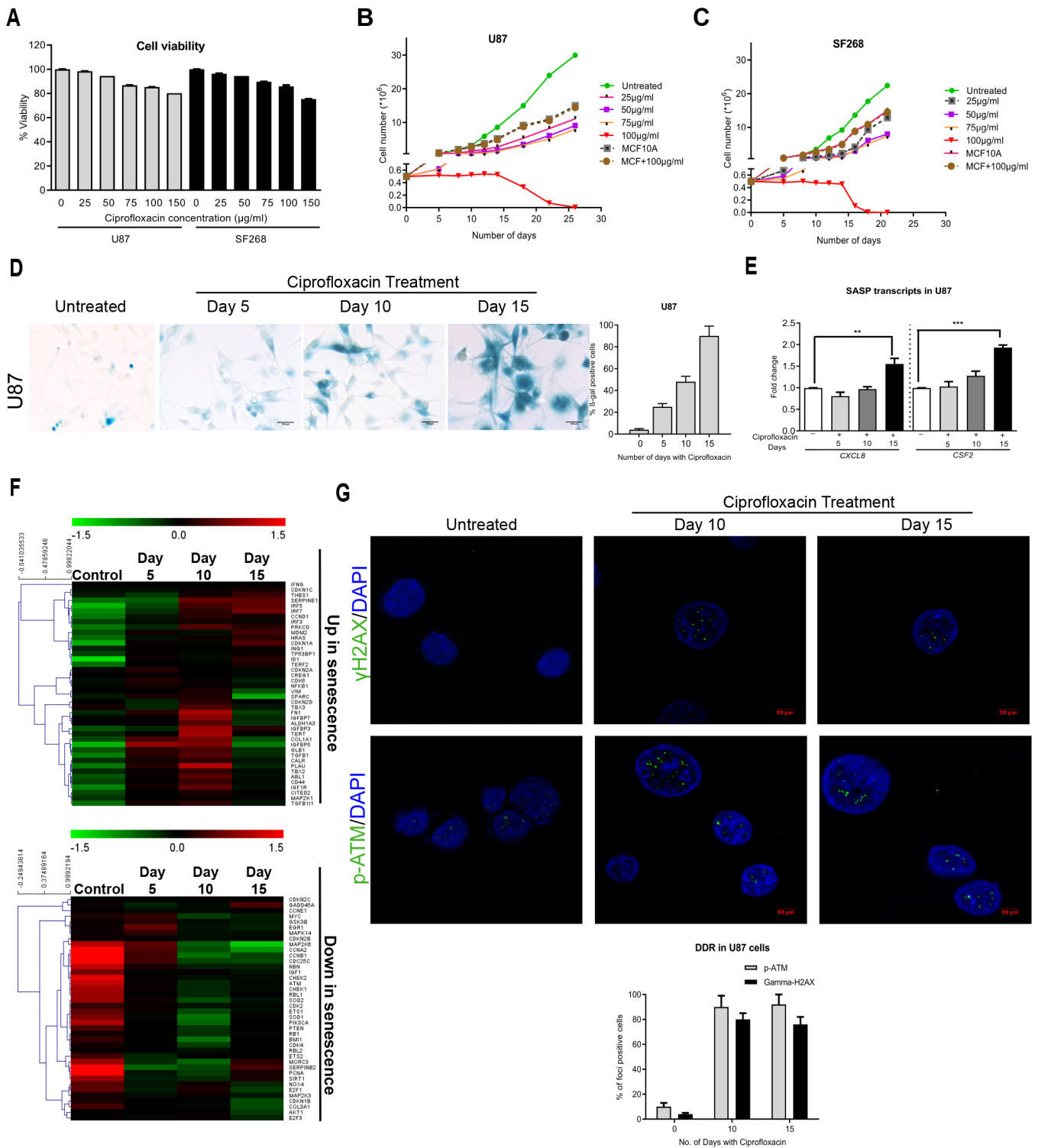


Fig. 1. Ciprofloxacin induces senescence of glioblastoma cells in concentration- and time-dependent manner. (A) Evaluation of cytotoxicity in cell lines as indicated after 48-hr treatment with ciprofloxacin, assessed using MTT assays. (B,C) Assessment of cell proliferation using Trypan Blue assay over 30 days in response to different concentrations of ciprofloxacin. Non-tumorigenic MCF10A cells were used for comparison. (D) Left: Representative images of senescent cells after treatment with ciprofloxacin for the durations indicated, detected by staining for SA-β-galactosidase. Scale bars: 100 µm. Right: Quantification of senescent U87 cells as shown on the left. Scale bars: 100 µm. (E) U87 cells were treated with ciprofloxacin for the indicated days, and expression levels of *CXCL8* and *CSF2* were quantified by real-time RT-PCR. Significance was calculated using Student's *t*-test. (F) Heat map showing the expression levels of genes associated with senescence in U87 cells treated with ciprofloxacin for 5, 10 or 15 days (U87 day5, U87 day10 or U87 day15, respectively) or left untreated (control). (G) Top: Representative immunofluorescence images, showing cells stained for γ-H2AX (green) and phosphorylated ATM (p-ATM, green) after treatment with ciprofloxacin for 10 or 15 days, and of untreated control cells. Nuclei were counterstained by DAPI (blue). Scale bars: 50 µm. Bottom: DNA damage response (DDR) in U87 cells in response to treatment with ciprofloxacin. Quantification of p-ATM and γ-H2AX levels during the same experiment. On average, 50 cells from each experiment were counted. Bar graphs represent mean±s.d.

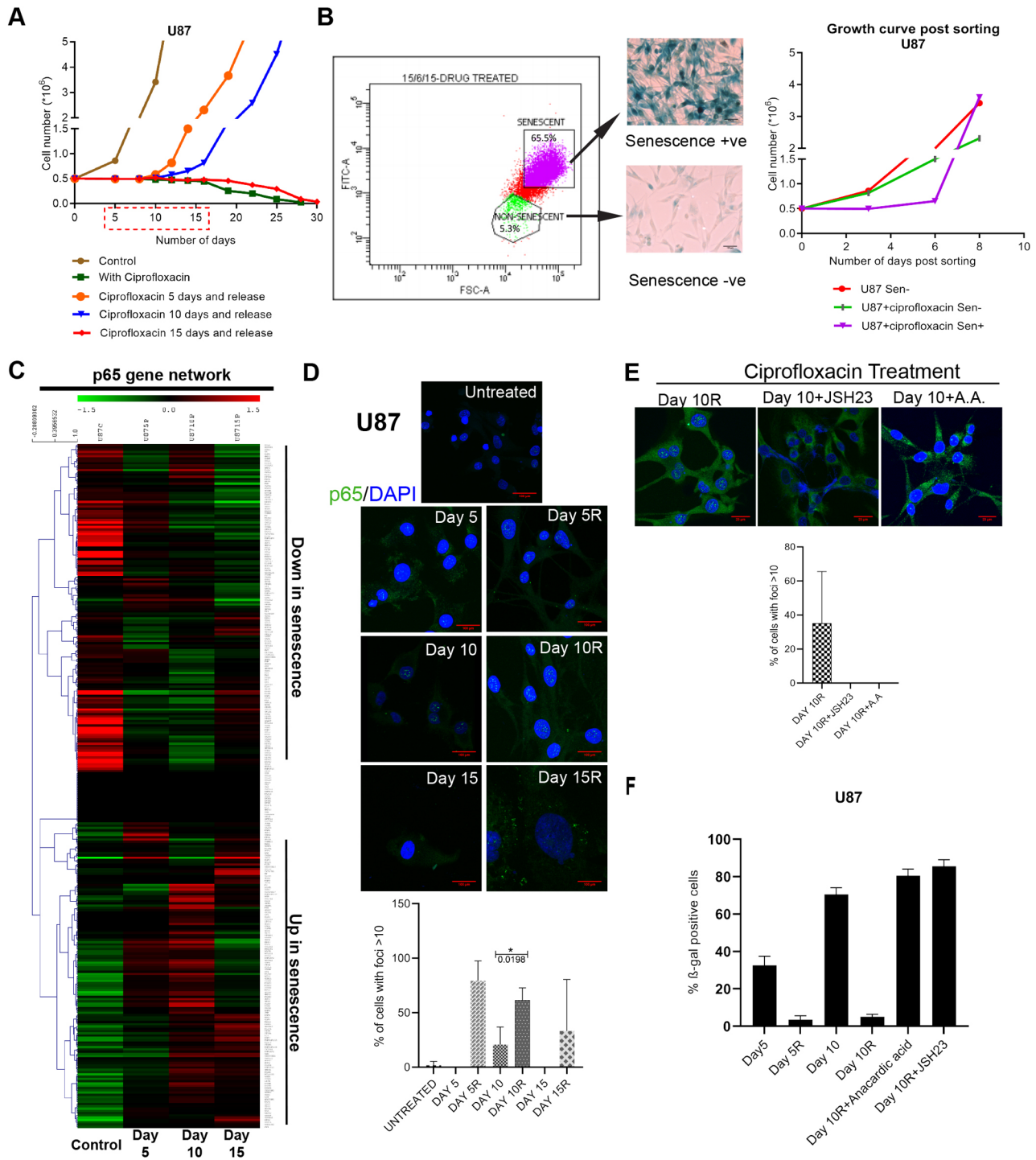


Fig. 2. Nuclear translocation of p65 reversed therapy-induced senescence. (A) Quantification of U87 cells treated with ciprofloxacin between 5 and 15 days, followed by culturing in ciprofloxacin-free medium for up to 30 days as indicated. Cell numbers were counted at indicated time points in the presence or absence of ciprofloxacin and after withdrawal of ciprofloxacin, showing an increase in cell numbers when ciprofloxacin treatment was stopped after 5 or 10 days. Cells were counted using a Trypan Blue assay. (B) Left: U87 cells at day 10 of ciprofloxacin treatment were sorted into senescent and non-senescent populations using FSC and FITC, then were reseeded and maintained in complete medium. Middle: representative images of senescence-positive and senescence-negative populations stained for SA- β -galactosidase. Right: cells were counted every 2 days until 8 days using a Trypan Blue assay. When re-cultured for up to 8 days in ciprofloxacin-free medium, both senescent (U87+ciprofloxacin Sen+) and non-senescent (U87+ciprofloxacin Sen-) cells were able to proliferate. Non-senescent U87 cells without previous ciprofloxacin treatment are shown as a control. Scale bars: 100 μ m. (C) Heat map showing the expression of different p65 network genes at days 5, 10 or 15 in ciprofloxacin-treated U87 parent cells (day 0, control). (D) Top: Images showing immunofluorescence staining for p65 (green) in U87 cells treated with ciprofloxacin for the days indicated and after ciprofloxacin withdrawal for 5 days (R). Nuclei were stained with DAPI (blue). Scale bars: 100 μ m. Bottom: Quantification of the images shown. Error bars indicate the mean+s.d. Significance was calculated using two-tailed paired Student's *t*-test. **P*<0.05. (E) Top: Immunofluorescence images of U87 cells stained for p65 (green) after treatment with ciprofloxacin for 10 days followed by culturing for further 5 days without ciprofloxacin (Day10R) and either with the p65 translocation inhibitor JSH23 (+JSH23) or with anacardic acid (+A.A). Nuclei were stained with DAPI (blue). Scale bars: 20 μ m. Bottom: Bar graph shows quantification of the percentage of cells with p65 foci for the indicated treatments. Bar graph represents the mean+s.d. (F) Quantification of SA- β -gal-positive cells under treatment conditions as indicated (*n*=3). Bar graph represents mean+s.d.

p16 were increased in day10R+anacardic acid cells and day15 cells compared to levels in day10 cells, suggesting p65 mediates rescue of ciprofloxacin-treated glioma cells from senescence by controlling ROS (Fig. S3F).

To further confirm that p65 nuclear translocation is necessary for cells to escape senescence, we used the inducible IKB α -mut (super repressor) (Boehm et al., 2007) to rescue the p65 nuclear translocation in response to treatment with ciprofloxacin. This doxycycline-inducible dominant-negative IKB phosphorylation mutant was expressed in day10R cells to sequester p65 in the cytoplasm, which resulted in cells being positive for SA- β -gal, similar to day10 ciprofloxacin treatment and pharmacological inhibition of p65 translocation, and in contrast to day10R cells (Fig. 3A,B). Further, we confirmed that nuclear translocated p65 was, indeed, transcriptionally active by using a luciferase-based NF κ B (p65 i.e. RELA) promoter reporter assay. The day10 ciprofloxacin-treated cells did not show any significant change in the NF κ B promoter activity. However, there was a 10-fold increase in NF κ B promoter activity in day10R cells, which significantly reduced in day15 cells. This surge of NF κ B promoter activity subsided in day10R cells in the presence of the IKB α -mut (super repressor) (Fig. 3C). These data confirm that nuclear translocation of p65 is required to reverse ciprofloxacin-induced senescence.

To check the reversibility of senescence *in vivo*, luciferase-labeled U87 cells were used. These cells were given the following treatments: ciprofloxacin for 10 days (day10), ciprofloxacin for 15 days (day15) and ciprofloxacin for 10 days followed by drug removal and addition of p65 inhibitor (JSH23) for 5 days (day10R+JSH23). The cells treated with ciprofloxacin for 10 days were flow sorted into senescence-positive (day10Sen+) and senescence-negative (day10Sen-) populations. All these cells with different treatments were orthotopically injected into the brain of CD-1 NUDE mice and monitored for tumor formation. The results show that both day10Sen+ and day10Sen- cells formed aggressive tumors compared to untreated U87 cells, whereas both day15 and day10R+JSH23 cells failed to form tumors in mice (Fig. 3D), confirming the existence of a window of reversibility for senescent cells *in vivo* that can be stopped by preventing p65 nuclear translocation using p65 translocation inhibitors.

Incremental increase of SMAD7 in senescent cells

To identify possible mechanisms responsible for the regulation of p65 translocation, we re-analyzed transcriptome data from senescent populations. An unbiased binary comparison of senescence time points identified differential gene expression in response to treatment with ciprofloxacin. The overlap of deregulated genes when comparing individual senescent time points (day5, 10 and 15) versus parent U87 cells revealed genes unique to each time point, and the overlap of these gene sets across all the groups yielded a total of 45 genes (Fig. 4A). Individual analysis of the 45 genes that overlap at all time points showed recurrent deregulation of SMAD family genes. Specifically, *SMAD7* showed an incremental pattern of expression over time in response to ciprofloxacin treatment (Fig. 4B). Real-time PCR of SMAD genes found an incremental upregulation of *SMAD7* mRNA between days 5 and 15 of ciprofloxacin treatment (Fig. 4C). Since *SMAD7* acts as an adaptor in the E3 ubiquitin–ligase complex (Kavsak et al., 2000), we wanted to explore whether nuclear *SMAD7* in senescent cells can mediate p65 degradation. Preliminary immunoprecipitation experiments of p65 from the nucleus of cells that contain low levels of *SMAD7* (day 0) and of senescent cells with high levels of

SMAD7 in their nucleus (day10 after treatment with ciprofloxacin) showed nuclear p65 to be 1.4-fold more ubiquitylated in the cells containing high levels of *SMAD7* (data not shown). This indicates ubiquitin-mediated degradation of nuclear p65 in the presence of *SMAD7* within senescent cells as a possible mechanism of senescence reversal; however, this observation needs thorough investigation with detailed experiments.

Therapy-induced senescence holds a promising solution for the treatment of different cancer types, including gliomas. Previously, glioma cells have been reported to undergo therapy-induced senescence in response to radiation-induced damage (Jeon et al., 2016; Kaur et al., 2015), ROS production (Colavitti and Finkel, 2005) and mitochondrial dysfunction (Passos et al., 2010), which is often associated with increased p65 activity (Chien et al., 2011; Ge et al., 2012). However, in our study we witnessed therapy-induced reversible senescence through a rare p65-induced proliferation phenotype, supporting a diverse role of p65 biology. Taken together, we show that ciprofloxacin-induced senescence in glioblastoma-derived cell lines can be divided into three stages, i.e. (1) initiation, (2) pseudo-senescence (reversible senescence) and (3) irreversible senescence. These senescence states are dynamic and molecularly distinct. Senescence, a tumor-suppressive mechanism, might be a promising alternative to cytotoxicity-inducing cancer therapy. However, the fact that we found therapeutic endpoint ‘senescence’ to be reversible until a certain time point has clinical implications, as premature drug withdrawal on the basis of the senescence phenotype might lead to disease recurrence. Thus, to understand what triggers pseudo-senescent cells towards irreversible senescence is therapeutically relevant. With prolonged ciprofloxacin treatment, senescent cells show high levels of *SMAD7*, ROS and DNA damage with loss of nuclear p65. Importantly, at this stage, if ciprofloxacin treatment is withdrawn, no nuclear translocation of p65 is seen, and cells stay senescent and eventually become apoptotic. Our results were also valid *in vivo*, within an orthotopic glioblastoma mouse model. To our best knowledge, this is the first report that identifies how temporal and spatial localization of p65 controls the dynamic (reversible and irreversible) states of ciprofloxacin-induced senescence (Fig. 4D). Accordingly, the combination of senotherapeutics and p65 nuclear translocation inhibitors can induce permanent senescence, preventing disease recurrence.

MATERIALS AND METHODS

Cell lines and cell culture

The MCF 10A non-tumorigenic epithelial cell line was kindly provided by Dr Amit Dutt (Advanced Centre for Treatment, Research and Education in Cancer, Kharghar, Navi Mumbai, India). U87 and SF268 human glioblastoma cell lines were from the American Type Culture Collection (ATCC). MCF 10A, U87MG and SF268 cell were grown at 37°C in a humidified 5% CO₂, 95% air atmosphere. MCF 10A cells were grown in DMEM-F-12 (Gibco) containing 15% fetal bovine serum (Gibco), 20 ng/ml epidermal growth factor (EGF; Sigma; cat. no. E9644), 10 μ g/ml wosulin (recombinant insulin; Wockhardt Pharma), 500 ng/ml hydrocortisone, 2000 μ g/ml streptomycin, 1000 units/ml penicillin and 50 μ g/ml amphotericin B. U87MG and SF268 cell lines were cultured in DMEM (Gibco) supplemented with 10% fetal bovine serum (Gibco), 2000 μ g/ml streptomycin, 50 μ g/ml of amphotericin B and 1000 units/ml penicillin. Cell lines were authenticated by STR profiling using the PROMEGA STR profiling kit, 10 markers and were mycoplasma tested.

Ethics approval and consent to participate

The study was approved by Tata Memorial Centre institutional ethics committee (TMC-IEC III) and was carried out in accordance with the Declaration of Helsinki. Informed consent was obtained from each patient prior to their inclusion in the study.

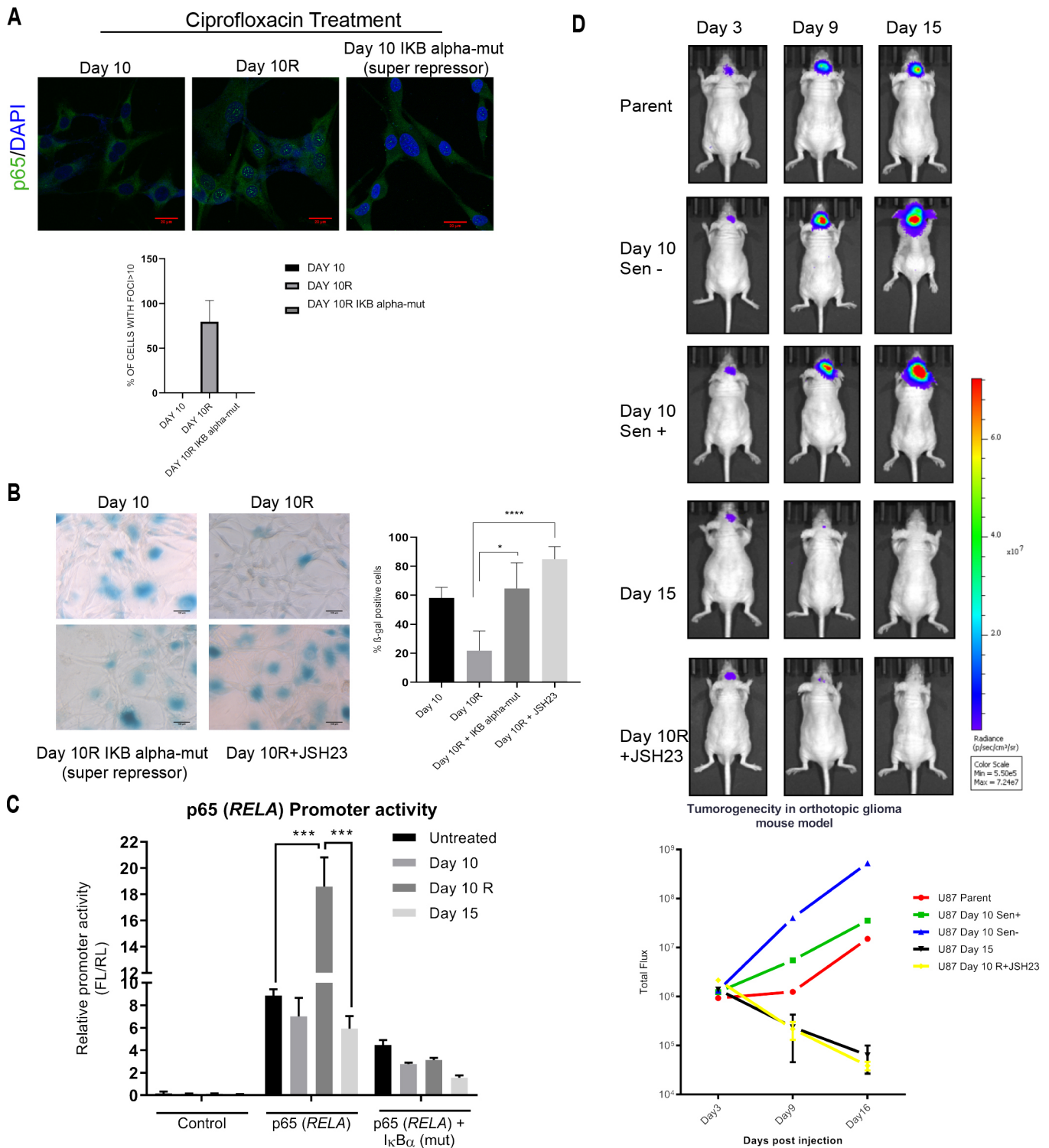


Fig. 3. Inhibition of p65 inhibits reversible senescence *in vitro* and *in vivo*. (A) Top: Immunofluorescence images of U87 cells stained for p65 at day 10 of ciprofloxacin treatment (Day 10), after ciprofloxacin withdrawal (Day10R) and after ciprofloxacin withdrawal with IκBα-mut (super repressor) (day10R IκBα-mut). Bottom: Bar graph represents quantification of percentage of cells with p65 foci, showing mean+s.d. Scale bars: 20 μm. (B) Left: SA-β-gal staining of U87 cells after ciprofloxacin treatment as indicated. Right: Bar graph represents mean+s.d. Significance was calculated using one-way ANOVA test. Scale bars: 100 μm. (C) NFκB p65 (RELA) transcriptional activity in ciprofloxacin-treated U87 cells. The NFκB firefly luciferase construct was transfected into untreated, Day10, Day10R, and Day15 ciprofloxacin-treated cells. As a control, Con A control plasmid was transfected together with the Renilla luciferase construct. The pTRIPZ IκBα construct was used to suppress NFκB. Luciferase values subsequent to normalization are plotted. Bar graph represents mean+s.d. Significance was calculated using two-tailed paired Student's *t*-test. (D) U87 cells expressing luciferase were injected orthotopically into CD1-NUDE mice. The total of five groups include control (parent), flow-sorted Day10 senescent cells (Day10 Sen+), Day10 non-senescent cells (Day10 Sen-), Day15 cells and Day10R+JSH23 cells. Top: Representative images of bioluminescence in mouse at different days post injection. Bottom: Quantification of bioluminescence from each group at the days indicated, showing tumor growth over time, based on total bioluminescence flux. Error bars show s.d. Significance was calculated using one-way ANOVA test. **P*<0.05; ****P*<0.001; *****P*<0.0001; ns, not significant.

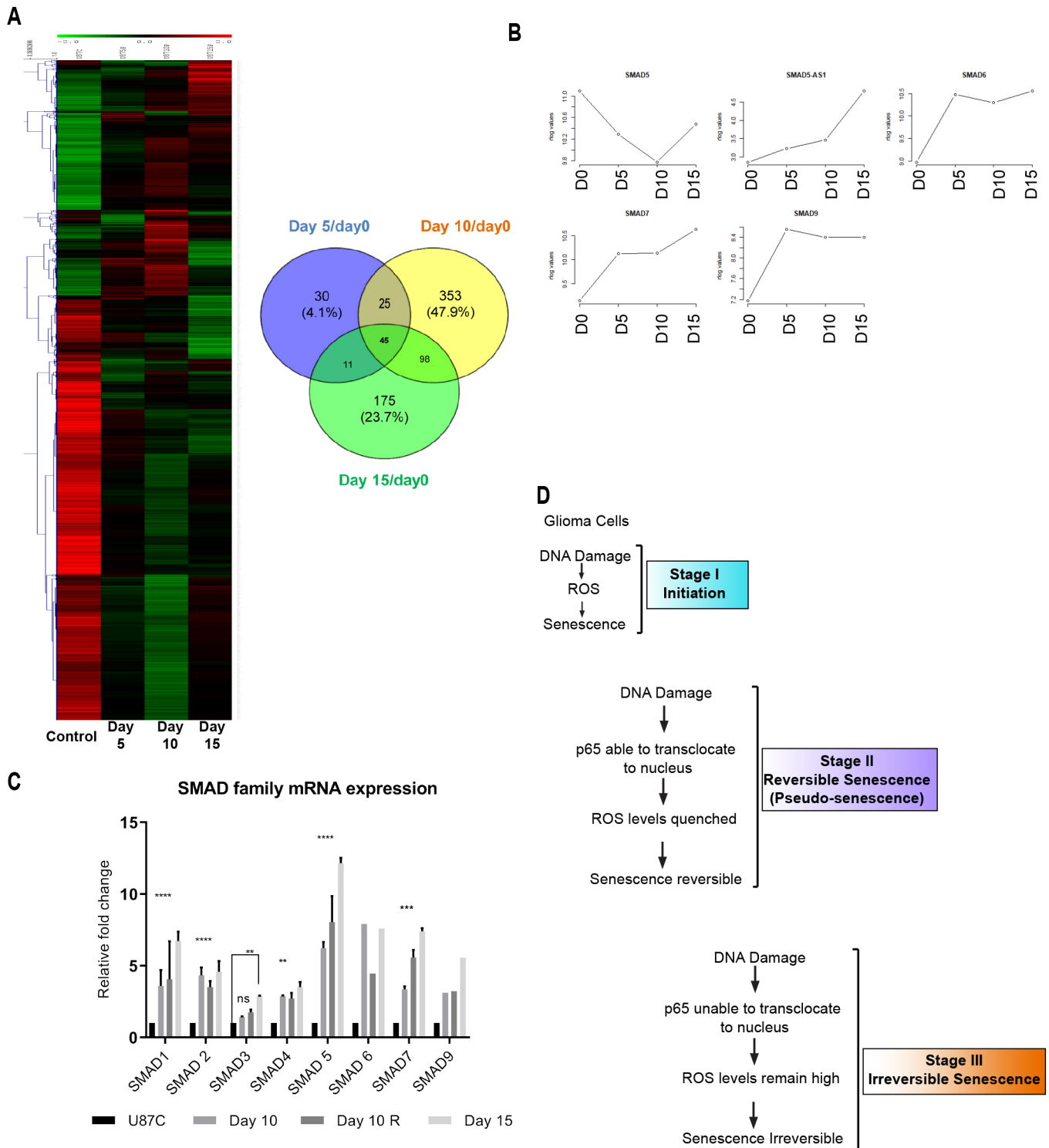


Fig. 4. SMAD7-mediated regulation of p53 translocation in pseudo-senescent glioblastoma cells. (A) Left: Heatmap of deregulated genes across parent U87 (control), day5, day10 and day15 ciprofloxacin treatment samples. Right: Venn diagram of genes deregulated in individual senescent time points versus parental U87 cells (day 0). (B) Gene expression patterns of significantly deregulated SMAD family genes across parent U87 (D0), day5 (D5), day10 (D10) and day15 (D15) ciprofloxacin treatment samples. The x-axes denote experimental time points and y-axes represent log expression values. (C) Quantification of SMAD family gene mRNA expression by real-time qPCR in U87 cells. Cells were left untreated (U87C), treated with ciprofloxacin for 10 or 15 days (Day 10 and Day 15, respectively) or treated with ciprofloxacin for 10 days before withdrawal for a further 5 days (Day 10R). Transcript levels were normalized against RPL16 (internal control) and mRNA levels of the respective SMAD genes in untreated U87 cells. Bar graph represents mean+s.d. Significance was calculated using two-way ANOVA. ** $P < 0.01$; *** $P < 0.001$; **** $P < 0.0001$; ns, not significant. (D) Model depicting the effect ciprofloxacin has on glioma cells, as well as the reversibility and irreversibility of the stages of senescence in time dependent manner.

Ciprofloxacin treatment

Ciprofloxacin was purchased from Sigma-Aldrich ($\geq 98\%$ HPLC). Stock solution of 3 mg/ml was made in autoclaved milli-Q water at pH 1.98.

MTT assay to assess cell proliferation

U87MG or SF268 cells were seeded into 96-well plates at a density of 5×10^3 cells per well, incubated for 24 h and exposed to the following concentration of ciprofloxacin: 25, 50, 75, 100 $\mu\text{g/ml}$. After 48 h incubation with different concentrations of ciprofloxacin, medium was removed from wells and MTT assay solution was added. Cells were incubated with MTT for 4–6 h. The crystals created after incubation were dissolved in DMSO (dimethyl sulfoxide). Absorbance of obtained colored solutions were measured at a wavelength of 570 nm. Each result was calculated from three independent measurements. Results of cell viability were presented in percent compared to control cells (100%). The results were presented as the means \pm s.e.m. All the graphs in this manuscript were plotted using GraphPad Prism software.

Trypan Blue assay

5×10^5 U87MG or SF268 cells were seeded into 6-well plates and incubated for 24 h in 10%. After 24 h, cells were exposed to the same concentrations of ciprofloxacin used for MTT assay for 25 days. Medium was removed after every 24 h and replaced with fresh medium containing appropriate concentrations of ciprofloxacin. Every 48 h, cells were trypsinized (0.05% trypsin containing 0.02% EDTA) and harvested in 1 ml of 10% DMEM. 10 μl of this cell suspension was mixed with an equal volume of Trypan Blue and counted in a haemocytometer chamber under inverted microscope at $10\times$ magnification. The number of viable cells calculated using the equation: $A/4 \times 2 \times 10^4 \times X$, with A = total number of viable cells, and X = volume of cell suspension (in ml). Results were obtained from three independent experiments and represented as mean \pm s.e.m. Significant difference of the mean values was determined using Student's *t*-test; $P < 0.05$ was considered significant.

Morphological changes

To assess morphological changes, 5×10^4 U87MG and SF268 cells were seeded in triplicates in a 6 well plate (NUNC). After incubation for 24 h, cells were treated with ciprofloxacin for 5, 10 or 15 days (100 $\mu\text{g/ml}$) and observed at $20\times$ magnification under a phase-contrast Olympus microscope. Data were processed using Q-capture pro software.

Reversibility and irreversibility of cell growth

5×10^4 U87MG and SF268 cells were seeded into three 6-well plates (Nunc) and treated with 100 $\mu\text{g/ml}$ ciprofloxacin for 5, 10 or 15 days. Treatment was given every 24 h by replacing old with fresh medium supplemented with ciprofloxacin. At the end of each treatment time, cells in three wells of each plate were placed in ciprofloxacin-free medium, whereas cells in the remaining three wells continued to receive ciprofloxacin. Cells were counted every 48 h using Trypan Blue assay, and cell numbers were compared between cells treated with ciprofloxacin and those grown in ciprofloxacin-free medium at time points specified.

Senescence associated- β -galactosidase activity assay

U87 and SF268 cells were seeded into 6-well plates and treated with 100 $\mu\text{g/ml}$ ciprofloxacin for 5, 10 or 15 days. Senescence Associated- β -galactosidase (SA- β -gal) activity assay was performed using a protocol published by Ghorai et al. (2020). Cells were viewed using a Leica microscope ($20\times$) and analyzed using Q-capture pro software. Cells stained blue were scored as being senescence positive for associated- β -galactosidase activity, and were quantified, expressed as a percent of the total number of cells and normalized against the background staining of untreated control cells. An average of ≥ 100 cells was calculated for each time point.

FACS sorting of live senescent cells

Flow cytometry was used for sorting of live senescent cells, on the basis of their size and autofluorescence. Cells of increased size and autofluorescence were scored as being senescence positive, whereas those of normal size and autofluorescence were scored as being senescence negative. (Hewitt et al., 2013; Martin-Ruiz et al., 2004; Passos and von Zglinicki, 2007)

Immunofluorescence

Cells were grown on glass coverslips to 60–70% confluence, fixed with methanol:acetic acid (3:1) for 15 min at room temperature and permeabilized with 0.25% Triton X-100 for 15 min at 4°C. Blocking was done using 1% bovine serum albumin for 1 h at room temperature, and primary antibody incubation was done overnight at 4°C. Upon secondary antibody incubation, coverslips were mounted onto glass slides using mounting solution containing DAPI (Invitrogen). Data acquisition was performed using a $63\times$ objective on LSM780 microscope equipped with FITC and TRITC filters. Images were captured and analyzed using LAS AF Live software (Leica) and processed using Adobe illustrator. To compare protein expression levels and localization, care was taken to ensure that images were taken with the same exposure time. To analyze foci images were processed using LSM Image Browser software and foci were counted using FociCounter software. The following proteins were assessed by immunofluorescence: γH2AX (s139) (CST kit#9947; dilution 1:400), p-ATM (s1981) (Abcam #ab19304; dilution 1:100), p65 (Abcam# ab16502; dilution 1:100), and F-actin (Invitrogen A12379 Phalloidin; dilution 1:100).

ROS analysis

ROS analysis was performed as described by Salunkhe et al. (2020b). Briefly, cells were incubated with 5 μM 2',7'-dichlorofluorescein (DCFDA) in $1\times$ PBS for 30 min in the dark. Cells were washed with PBS three times and analyzed to detect DCFDA fluorescence by using an FL1 filter (FACS Caliber).

Quantitative real-time PCR

Quantitative real-time PCR (qPCR) was performed as described by Salunkhe et al. (2018). RNA was extracted from U87 and SF268 cells treated with 100 $\mu\text{g/ml}$ ciprofloxacin for 5, 10 or 15 days using the Trizol Method. Significance of difference was analyzed using Student's *t*-test. Data represent the mean \pm s.d. of three biological replicates done in duplicates.

Orthotopic xenograft mouse experiments

All the animals were bred and maintained according to protocols issued by the Laboratory Animal Facility of ACTREC-TMC. Protocols were reviewed by the Institutional Animal Ethics Committee (IAEC). For detailed protocols refer to Rajendra et al., (2018). pLenti CMV Puro LUC (w168-1) was a gift from Eric Campeau and Paul Kaufman (Addgene plasmid #17477). In brief, NUDE/SCID mice (male, 6–8 weeks old) were injected with 1×10^5 pLenti CMV Puro LUC (w168-1) in U87 cells pretreated with ciprofloxacin and in combination with JSH23 for different days (days 5, 10 or 15) were injected intracranially. Tumors were imaged on different days post injection, luciferin signal were defined using Living Image software, and the total photons/s/ (photons per second) was recorded.

Bioluminescence imaging

Mice were anaesthetized with 2% isoflurane mixed with O_2 and administered luciferin (D-Luciferin potassium salt, 150 mg/kg, Calliper Life Sciences) through intraperitoneal injection. Images were acquired 10–12 minutes after injection. The time chosen was based on the pharmacokinetics of luciferin, which defines that maximum luminescence emission and greatest sensitivity of detection is obtained when cell luminescence is detected after 10–15 min of injection of luciferin. The imaging parameters were constant across all the mice groups. Regions of interest encompassing the intracranial signal area were defined using Living Image software, and the total number of photons was recorded per second per steradian per square cm (s/sr/cm²).

Inducible IkappaB super repressor

U87 cells were transfected with the inducible IKBalpa-mut super repressor. The pBabe-Puro-IKBalpa-mut (super repressor) plasmid used was a gift from Dr Prasanna Venkatraman (Advanced Centre for Treatment, Research and Education in Cancer, Tata Memorial Centre, Navi Mumbai, India). Cells were then treated with ciprofloxacin, and doxycycline was used in day 10R cells to induce the dominant-negative phosphorylation mutant of Ikb, whose two point mutations S32A and S36A yielded the 'super-repressor' allele, the protein product of which is resistant to phosphorylation

and degradation. These cells were then compared for translocation of p65 and b-gal activity with untransfected day 10R cells.

p65 inhibitor studies

Ciprofloxacin-treated cells were treated with either JSH23 (cat. No. 481408, Sigma) 10 μ M for 5 more days or Anacardic acid (200 μ M, Abcam ab120892) on day 10 release (day10R) cells together with an appropriate control cell population.

Quantification of transcripts and differential genes analysis

Differential gene analysis was performed through a gene expression analysis pipeline adopted in our laboratory (Salunkhe et al., 2020a). Quantification of transcript levels was carried out using the Salmon software tool version v0.8.1 (Patro et al., 2017) on raw FASTQ RNA-seq data. Transcriptome index building was performed using the transcriptome reference index downloaded from the UCSC browser [University of California Santa Cruz *Homo sapiens* reference genome (build hg19) GTF file] followed by quantification of transcripts. Further downstream analysis of differential gene identification was carried out by using DESeq2 R Bioconductor package (Love et al., 2014) that uses negative binomial generalized linear models. Transcript abundance files from Salmon were imported and converted to gene level information, and carried out by using the tximport R Bioconductor package (Soneson et al., 2015). Low-count genes were removed before running DESeq2 function and all possible class comparisons were carried out. Log-fold changes and *P*-values (Wald test) were calculated for each gene for each comparison. Genes were referred to as differential if Wald test values were $P < 0.05$ and met the $+2 < \log_2 FC < -2$ criteria. The regularized logarithm (rlog) method was used to transform and normalize the data, and processed values were used for clustering of genes in heatmaps.

NFkB promoter activity assay

To measure NFkB promoter activity, U87 cells were transiently transfected with NFkB-pGL4-luc2 and pGL4-hrl (5:1 ratio), or NFkB-pGL4-luc2 and pTRIPZ Ikb α , and the fold change in relative promoter activity (treated versus untreated) was calculated as a ratio of firefly luciferase to Renilla luciferase (FL:RL) activity. The constructs were kind gifts from Dr Prasanna Venkatraman, ACTREC. FL and RL activities were measured using the Dual luciferase assay system (Promega) and the readings were recorded in a Berthold luminometer for periods of 1 s.

AnnexinV-propidium iodide staining

To assess the mode of cell death in ciprofloxacin-treated cells at day 15, we stained for Annexin V surface labeling using the Annexin V-FITC early apoptosis detection kit, as per the manufacturer's instructions (Cell Signaling Technology, #6592). Treated cells and untreated (control) cells were resuspended in 96 μ l 1 \times Annexin V-binding buffer and incubated on ice with 1 μ l Annexin V-FITC conjugate for 10 min. This suspension was diluted to a final volume of 250 μ l with ice-cold 1 \times Annexin V-binding buffer and used immediately on an AttuneNxT flow cytometer. Data analysis was performed using FlowJo software.

Statistical analysis

All experiments were done in three independent biological replicates, unless stated otherwise in the figure legend. Significant difference was calculated using GraphPad software in-built two-tailed Student's *t*-test or ANOVA analysis. Results were considered significant in all experiments at $P < 0.05$. When representing quantitative data, significance levels were * $P < 0.05$, ** $P < 0.01$, *** $P < 0.001$ and **** $P < 0.0001$.

Acknowledgements

We thank Dr Amit Dutt (Integrated Genomics Laboratory, Advanced Centre for Treatment, Research and Education in Cancer, Tata Memorial Centre, Navi Mumbai, India) for providing MCF 10A cells and EGF, and Dr Prasanna Venkatraman (Advanced Centre for Treatment, Research and Education in Cancer, Tata Memorial Centre, Navi Mumbai, India) for pBabe-Puro-IKBA α -mut (super repressor).

Competing interests

The authors declare no competing or financial interests.

Author contributions

Conceptualization: S. Salunkhe, S.D.; Methodology: S. Salunkhe, S.V.M., J.N., S.D.; Validation: S. Salunkhe, S.V.M., J.N.; Formal analysis: S. Salunkhe, S.V.M., S.D.; Investigation: S. Salunkhe, S.V.M., J.N., S. Shah, N.G., R.T., D.S., J.R., E.K.; Resources: S.D.; Data curation: S. Salunkhe, S.D.; Writing - original draft: S. Salunkhe; Writing - review & editing: S. Salunkhe, S.V.M., S.D.; Visualization: S. Salunkhe, S.D.; Supervision: S.D.; Project administration: S.D.; Funding acquisition: S.D.

Funding

S.D. was funded by Department of Biotechnology (DBT), Govt. of India (grant number: BT/PR13863/MED/122/6/2016). S.S. and J.N. are CSIR fellows, S.V.M. and E.K. are DBT fellows.

Supplementary information

Supplementary information available online at <https://jcs.biologists.org/lookup/doi/10.1242/jcs.253203.supplemental>

Peer review history

The peer review history is available online at <https://jcs.biologists.org/lookup/doi/10.1242/jcs.253203.reviewer-comments.pdf>

References

- Aranha, O., Grignon, R., Fernandes, N., McDonnell, T. J., Wood, D. P. and Sarkar, F. H. (2003). Suppression of human prostate cancer cell growth by ciprofloxacin is associated with cell cycle arrest and apoptosis. *Int. J. Oncol.* **22**, 787-794. doi:10.3892/ijo.22.4.787
- Beauséjour, C. M., Krtolica, A., Galimi, F., Narita, M., Lowe, S. W., Yaswen, P. and Campisi, J. (2003). Reversal of human cellular senescence: roles of the p53 and p16 pathways. *EMBO J.* **22**, 4212-4222. doi:10.1093/emboj/cdg417
- Boehm, J. S., Zhao, J. J., Yao, J., Kim, S. Y., Firestein, R., Dunn, I. F., Sjöström, S. K., Garraway, L. A., Weremowicz, S., Richardson, A. L. et al. (2007). Integrative genomic approaches identify IKBKE as a breast cancer oncogene. *Cell* **129**, 1065-1079. doi:10.1016/j.cell.2007.03.052
- Chang, B. D., Broude, E. V., Dokmanovic, M., Zhu, H., Ruth, A., Xuan, Y., Kandel, E. S., Lausch, E., Christov, K. and Roninson, I. B. (1999). A senescence-like phenotype distinguishes tumor cells that undergo terminal proliferation arrest after exposure to anticancer agents. *Cancer Res.* **59**, 3761-3767.
- Chang, B.-D., Swift, M. E., Shen, M., Fang, J., Broude, E. V. and Roninson, I. B. (2002). Molecular determinants of terminal growth arrest induced in tumor cells by a chemotherapeutic agent. *Proc. Natl. Acad. Sci. USA* **99**, 389-394. doi:10.1073/pnas.012602599
- Chen, A. Y. and Liu, L. F. (1994). DNA topoisomerases: essential enzymes and lethal targets. *Annu. Rev. Pharmacol. Toxicol.* **34**, 191-218. doi:10.1146/annurev.pa.34.040194.001203
- Chen, C.-R., Malik, M., Snyder, M. and Drlica, K. (1996). DNA gyrase and topoisomerase IV on the bacterial chromosome: quinolone-induced DNA cleavage. *J. Mol. Biol.* **258**, 627-637. doi:10.1006/jmbi.1996.0274
- Chen, J.-H., Hales, C. N. and Ozanne, S. E. (2007). DNA damage, cellular senescence and organismal ageing: causal or correlative? *Nucleic Acids Res.* **35**, 7417-7428. doi:10.1093/nar/gkm681
- Chien, Y., Scupp, C., Wang, X., Fang, X., Balgley, B., Bolden, J. E., Premsrirut, P., Luo, W., Chicas, A., Lee, C. S. et al. (2011). Control of the senescence-associated secretory phenotype by NF- κ B promotes senescence and enhances chemosensitivity. *Genes Dev.* **25**, 2125-2136. doi:10.1101/gad.172767.11
- Colavitti, R. and Finkel, T. (2005). Reactive oxygen species as mediators of cellular senescence. *IUBMB Life* **57**, 277-281. doi:10.1080/15216540500091890
- Di Micco, R., Fumagalli, M., Cicala, A., Piccinin, S., Gasparini, P., Luise, C., Schurra, C., Garre', M., Giovanni Nuciforo, P., Bensimon, A. et al. (2006). Oncogene-induced senescence is a DNA damage response triggered by DNA hyper-replication. *Nature* **444**, 638-642. doi:10.1038/nature05327
- Ditch, S. and Paull, T. T. (2012). The ATM protein kinase and cellular redox signaling: beyond the DNA damage response. *Trends Biochem. Sci.* **37**, 15-22. doi:10.1016/j.tibs.2011.10.002
- Duy, C., Teater, M., Garrett-Bakelman, F. E., Carroll, M. and Melnick, A. (2016). Acute myeloid leukemia cells resist chemotherapy through a reversible senescence-like state maintaining repopulation potential. *Blood* **128**, 582-582. doi:10.1182/blood.V128.22.582.582
- Elmore, L. W., Di, X., Dumur, C., Holt, S. E. and Gewirtz, D. A. (2005). Evasion of a single-step, chemotherapy-induced senescence in breast cancer cells: implications for treatment response. *Clin. Cancer Res.* **11**, 2637-2643. doi:10.1158/1078-0432.CCR-04-1462
- Ewald, J. A. and Jarrard, D. F. (2012). Decreased skp2 expression is necessary but not sufficient for therapy-induced senescence in prostate cancer. *Transl. Oncol.* **5**, 278-287. doi:10.1593/tlo.12181

- Ewald, J. A., Desotelle, J. A., Wilding, G. and Jarrard, D. F. (2010). Therapy-induced senescence in cancer. *J. Natl. Cancer Inst.* **102**, 1536-1546. doi:10.1093/jnci/djq364
- Fumagalli, M., Rossiello, F., Clerici, M., Barozzi, S., Cittaro, D., Kaplunov, J. M., Bucci, G., Dobreva, M., Matti, V., Beausejour, C. M. et al. (2012). Telomeric DNA damage is irreparable and causes persistent DNA-damage-response activation. *Nat. Cell Biol.* **14**, 355-365. doi:10.1038/ncb2466
- Ge, H., Ni, S., Wang, X., Xu, N., Liu, Y., Wang, X., Wang, L., Song, D., Song, Y. and Bai, C. (2012). Dexamethasone reduces sensitivity to cisplatin by blunting p53-dependent cellular senescence in non-small cell lung cancer. *PLoS ONE* **7**, e51821. doi:10.1371/journal.pone.0051821
- Georger, B., Bourdeaut, F., DuBois, S. G., Fischer, M., Geller, J. I., Gottardo, N. G., Marabelle, A., Pearson, A. D. J., Modak, S., Cash, T. et al. (2017). A phase I study of the CDK4/6 inhibitor ribociclib (LEE011) in pediatric patients with malignant rhabdoid tumors, neuroblastoma, and other solid tumors. *Clin. Cancer Res.* **23**, 2433-2441. doi:10.1158/1078-0432.CCR-16-2898
- Ghorai, A., Mahaddalkar, T., Thorat, R. and Dutt, S. (2020). Sustained inhibition of PARP-1 activity delays glioblastoma recurrence by enhancing radiation-induced senescence. *Cancer Lett.* **490**, 44-53. doi:10.1016/j.canlet.2020.06.023
- Goldman, J. W., Shi, P., Reck, M., Paz-Ares, L., Koustenis, A. and Hurt, K. C. (2016). Treatment rationale and study design for the JUNIPER study: a randomized phase III study of abemaciclib with best supportive care versus erlotinib with best supportive care in patients with stage IV non-small-cell lung cancer with a detectable KRAS mutation whose disease has progressed after platinum-based chemotherapy. *Clin. Lung Cancer* **17**, 80-84. doi:10.1016/j.clc.2015.08.003
- Herbig, U. and Sedivy, J. M. (2006). Regulation of growth arrest in senescence: telomere damage is not the end of the story. *Mech. Ageing Dev.* **127**, 16-24. doi:10.1016/j.mad.2005.09.002
- Hewitt, G., von Zglinicki, T. and Passos, J. F. (2013). Cell sorting of young and senescent cells. *Methods Mol. Biol.* **1048**, 31-47. doi:10.1007/978-1-62703-556-9_4
- Jeon, H.-Y., Kim, J.-K., Ham, S. W., Oh, S.-Y., Kim, J., Park, J.-B., Lee, J.-Y., Kim, S.-C. and Kim, H. (2016). Irradiation induces glioblastoma cell senescence and senescence-associated secretory phenotype. *Tumour Biol.* **37**, 5857-5867. doi:10.1007/s13277-015-4439-2
- Kaur, E., Rajendra, J., Jadhav, S., Shridhar, E., Goda, J. S., Moiyadi, A. and Dutt, S. (2015). Radiation-induced homotypic cell fusions of innately resistant glioblastoma cells mediate their sustained survival and recurrence. *Carcinogenesis* **36**, 685-695. doi:10.1093/carcin/bgv050
- Kaur, E., Sahu, A., Hole, A. R., Rajendra, J., Chaubal, R., Gardi, N., Dutt, A., Moiyadi, A., Krishna, C. M. and Dutt, S. (2016). Unique spectral markers discern recurrent Glioblastoma cells from heterogeneous parent population. *Sci. Rep.* **6**, 26538. doi:10.1038/srep26538
- Kaur, E., Goda, J. S., Ghorai, A., Salunkhe, S., Shetty, P., Moiyadi, A. V., Sridhar, E., Mahajan, A., Jalali, R. and Dutt, S. (2019). Molecular features unique to glioblastoma radiation resistant residual cells may affect patient outcome - a short report. *Cell. Oncol.* **42**, 107-116. doi:10.1007/s13402-018-0411-7
- Kaur, E., Nair, J., Ghorai, A., Mishra, S. V., Achareker, A., Ketkar, M., Sarkar, D., Salunkhe, S., Rajendra, J., Gardi, N. et al. (2020). Inhibition of SETMAR - H3K36me2 - NHEJ repair axis in residual disease cells prevents glioblastoma recurrence. *Neuro Oncol.* **22**, 1785-1796. doi:10.1093/neuonc/noaa128
- Kavak, P., Rasmussen, R. K., Causing, C. G., Bonni, S., Zhu, H., Thomsen, G. H. and Wrana, J. L. (2000). Smad7 binds to Smurf2 to form an E3 ubiquitin ligase that targets the TGF β receptor for degradation. *Mol. Cell* **6**, 1365-1375. doi:10.1016/S1097-2765(00)00134-9
- Kloskowski, T., Gurtowska, N., Olkowska, J., Nowak, J. M., Adamowicz, J., Tworkiewicz, J., Dębski, R., Grzanka, A. and Drewa, T. (2012). Ciprofloxacin is a potential topoisomerase II inhibitor for the treatment of NSCLC. *Int. J. Oncol.* **41**, 1943-1949. doi:10.3892/ijo.2012.1653
- Lawless, C., Wang, C., Jurk, D., Merz, A., Zglinicki, T. and Passos, J. F. (2010). Quantitative assessment of markers for cell senescence. *Exp. Gerontol.* **45**, 772-778. doi:10.1016/j.exger.2010.01.018
- Lee, S. and Schmitt, C. A. (2019). The dynamic nature of senescence in cancer. *Nat. Cell Biol.* **21**, 94-101. doi:10.1038/s41556-018-0249-2
- Love, M. I., Huber, W. and Anders, S. (2014). Moderated estimation of fold change and dispersion for RNA-seq data with DESeq2. *Genome Biol.* **15**, 550. doi:10.1186/s13059-014-0550-8
- Martin-Ruiz, C., Saretzki, G., Petrie, J., Ladhoff, J., Jayapalan, J., Wei, W., Sedivy, J. and von Zglinicki, T. (2004). Stochastic variation in telomere shortening rate causes heterogeneity of human fibroblast replicative life span. *J. Biol. Chem.* **279**, 17826-17833. doi:10.1074/jbc.M311980200
- Miclau, T., Edin, M. L., Lester, G. E., Lindsey, R. W. and Dahners, L. E. (1998). Effect of ciprofloxacin on the proliferation of osteoblast-like MG-63 human osteosarcoma cells in vitro. *J. Orthop. Res.* **16**, 509-512. doi:10.1002/jor.1100160417
- Morgan, M. J. and Liu, Z.-G. (2011). Crosstalk of reactive oxygen species and NF- κ B signaling. *Cell Res.* **21**, 103-115. doi:10.1038/cr.2010.178
- Passos, J. F. and von Zglinicki, T. (2007). Methods for cell sorting of young and senescent cells. *Methods Mol. Biol.* **371**, 33-44. doi:10.1007/978-1-59745-361-5_4
- Passos, J. F., Nelson, G., Wang, C., Richter, T., Simillion, C., Proctor, C. J., Miwa, S., Olijslagers, S., Hallinan, J., Wipat, A. et al. (2010). Feedback between p21 and reactive oxygen production is necessary for cell senescence. *Mol. Syst. Biol.* **6**, 347. doi:10.1038/msb.2010.5
- Patro, R., Duggal, G., Love, M. I., Irizarry, R. A. and Kingsford, C. (2017). Salmon provides fast and bias-aware quantification of transcript expression. *Nat. Methods* **14**, 417-419. doi:10.1038/nmeth.4197
- Quick, Q. A. and Gewirtz, D. A. (2006). An accelerated senescence response to radiation in wild-type p53 glioblastoma multiforme cells. *J. Neurosurg.* **105**, 111-118. doi:10.3171/jns.2006.105.1.111
- Rajendra, J., Datta, K. K., Ud Din Farooqee, S. B., Thorat, R., Kumar, K., Gardi, N., Kaur, E., Nair, J., Salunkhe, S., Patkar, K. et al. (2018). Enhanced proteasomal activity is essential for long term survival and recurrence of innately radiation resistant residual glioblastoma cells. *Oncotarget* **9**, 27667-27681. doi:10.18632/oncotarget.25351
- Roberson, R. S., Kussick, S. J., Vallieres, E., Chen, S.-Y. J. and Wu, D. Y. (2005). Escape from therapy-induced accelerated cellular senescence in p53-null lung cancer cells and in human lung cancers. *Cancer Res.* **65**, 2795-2803. doi:10.1158/0008-5472.CAN-04-1270
- Saleh, T., Tyutyunyk-Massey, L. and Gewirtz, D. A. (2019). Tumor cell escape from therapy-induced senescence as a model of disease recurrence after dormancy. *Cancer Res.* **79**, 1044-1046. doi:10.1158/0008-5472.CAN-18-3437
- Salunkhe, S., Mishra, S. V., Nair, J., Ghosh, S., Choudhary, N., Kaur, E., Shah, S., Patkar, K., Anand, D., Khattry, N. et al. (2018). Inhibition of novel GCN5-ATM axis restricts the onset of acquired drug resistance in leukemia. *Int. J. Cancer* **142**, 2175-2185. doi:10.1002/ijc.31242
- Salunkhe, S., Chandran, N., Chandrani, P., Dutt, A. and Dutt, S. (2020a). CytoPred: 7-gene pair metric for AML cytogenetic risk prediction. *Brief. Bioinform.* **21**, 348-354. doi:10.1093/bib/bby100
- Salunkhe, S., Mishra, S. V., Ghorai, A., Hole, A., Chandrani, P., Dutt, A., Chilakapati, M. and Dutt, S. (2020b). Metabolic rewiring in drug resistant cells exhibit higher OXPHOS and fatty acids as preferred major source to cellular energetics. *Biochim. Biophys. Acta (BBA) Bioenerg.* **1861**, 148300. doi:10.1016/j.bbabi.2020.148300
- Schäfer, R., Karbach, D. and Hoppe, J. (1998). Multiple intracellular pathways interfere with the activation of a CPP32-like protease induced by serum deprivation of AKR-2B cells. *Exp. Cell Res.* **240**, 28-39. doi:10.1006/excr.1997.3928
- Schmitt, C. A. (2018). UnSASPing senescence: unmasking tumor suppression? *Cancer Cell* **34**, 6-8. doi:10.1016/j.ccell.2018.06.009
- Schmitt, C. A., Fridman, J. S., Yang, M., Lee, S., Baranov, E., Hoffman, R. M. and Lowe, S. W. (2002). A senescence program controlled by p53 and p16INK4a contributes to the outcome of cancer therapy. *Cell* **109**, 335-346. doi:10.1016/S0092-8674(02)00734-1
- Seay, T. M., Peretsman, S. J. and Dixon, P. S. (1996). Inhibition of human transitional cell carcinoma in vitro proliferation by fluoroquinolone antibiotics. *J. Urol.* **155**, 757-762. doi:10.1016/S0022-5347(01)66516-9
- Shiloh, Y. and Ziv, Y. (2013). The ATM protein kinase: regulating the cellular response to genotoxic stress, and more. *Nat. Rev. Mol. Cell Biol.* **14**, 197-210. doi:10.1038/nrm3546
- Somekh, E., Douer, D., Shaked, N. and Rubinstein, E. (1989). In vitro effects of ciprofloxacin and pefloxacin on growth of normal human hematopoietic progenitor cells and on leukemic cell lines. *J. Pharmacol. Exp. Ther.* **248**, 415-418.
- Soneson, C., Love, M. I. and Robinson, M. D. (2015). Differential analyses for RNA-seq: transcript-level estimates improve gene-level inferences. *F1000Res.* **4**, 1521. doi:10.12688/f1000research.7563.1
- Turner, N. C., Ro, J., André, F., Loi, S., Verma, S., Iwata, H., Harbeck, N., Loibl, S., Huang Bartlett, C., Zhang, K. et al. (2015). Palbociclib in Hormone-Receptor-Positive Advanced Breast Cancer. *N. Engl. J. Med.* **373**, 209-219. doi:10.1056/NEJMoa1505270
- Wang, L., Leite, de Oliveira, R., Wang, C., Fernandes Neto, J. M., Mainardi, S., Evers, B., Liefink, C., Morris, B., Jochems, F. et al. (2017). High-throughput functional genetic and compound screens identify targets for senescence induction in cancer. *Cell Rep.* **21**:773-783. doi:10.1016/j.celrep.2017.09.085
- Xue, W., Zender, L., Miething, C., Dickins, R. A., Hernandez, E., Krizhanovskiy, V., Cordon-Cardo, C. and Lowe, S. W. (2007). Senescence and tumour clearance is triggered by p53 restoration in murine liver carcinomas. *Nature* **445**, 656-660. doi:10.1038/nature05529
- Zhang, Y. and Yang, J.-M. (2011). The impact of cellular senescence in cancer therapy: is it true or not? *Acta Pharmacol. Sin.* **32**, 1199-1207. doi:10.1038/aps.2011.108